Astron. Astrophys. 364, 467–478 (2000)

ASTRONOMY AND ASTROPHYSICS

The broken light curves of gamma-ray bursts GRB 990123 and GRB 990510

S. Holland[1], **G. Björnsson**[2], **J. Hjorth**[3], **and B. Thomsen**[1]

[1] Aarhus Universitet, Institut for Fysik og Astronomi (IFA), Ny Munkegade, Bygning 520, 8000 Århus C, Denmark (holland@ifa.au.dk, bt@ifa.au.dk)
[2] University of Iceland, Science Institute, Dunhaga 3, 107 Reykjavik, Iceland (gulli@raunvis.hi.is)
[3] University of Copenhagen, Astronomical Observatory, Juliane Maries Vej 30, 2100 Copenhagen Ø, Denmark (jens@astro.ku.dk)

Received 9 June 2000 / Accepted 17 September 2000

Abstract. We have collected all of the published photometry for GRB 990123 and GRB 990510, the first two gamma-ray bursts where breaks were seen in the light curves of their optical afterglows, and determined the shapes of their light curves and the break times. These parameters were used to investigate the physical mechanisms responsible for the breaks and the nature of the ambient medium that the bursts occurred in. The light curve for GRB 990123 is best fit by a broken power law with a break 1.68 ± 0.19 days after the burst, a slope of $\alpha_1 = -1.12 \pm 0.08$ before the break, and a slope of $\alpha_2 = -1.69 \pm 0.06$ after the break. This is consistent with a collimated outflow with a fixed opening angle of $\theta_0 \approx 5^\circ$. In this case the break in the light curve is due to the relativistic fireball slowing to $\Gamma \approx 1/\theta_0$. The light curve for GRB 990510 is best fit by a continuous function with an early-time slope of $\alpha_1 = -0.54 \pm 0.14$, a late-time slope of $\alpha_2 = -1.98 \pm 0.19$, and a slow transition between the two regimes approximately one day after the burst. This is consistent with a collimated outflow with $\theta_0 \approx 5^\circ$ that is initially radiative, but undergoes a sideways expansion that begins approximately one day after the burst. This sideways expansion is responsible for the slow break in the light curve.

Key words: gamma rays: bursts

1. Introduction

In the first few months of 1999 bright optical afterglows (OAs) were observed for two gamma-ray bursts (GRBs): GRB 990123 and GRB 990510. Extensive follow-up observations were made at optical wavelengths for both GRBs, so it was possible to follow their light curves down to $V \approx 28$, with the deepest photometry being done with the *Hubble Space Telescope* (*HST*). These data, when put onto a common photometric system, can be used to constrain the shape of each burst's light curve. The resulting shape parameters (the time of the break, and the slopes before and after the break) can be used to constrain physical models of the OA, and the interaction of the relativistic ejecta from the initial blast with the surrounding medium.

Send offprint requests to: Stephen Holland

At 9:46:56.12 UT on 1999 January 23 the Burst and Transient Source Experiment (BATSE) detectors on the *Compton Gamma Ray Observatory* satellite detected GRB 990123 in the constellation Boötes. X-ray observations from the Dutch–Italian satellite *BeppoSAX* localized the position of the burst to within $5'$ (Piro 1999) and the Robotic Optical Transient Search Experiment (Akerlof & McKay 1999; Akerlof et al. 1999) detected an OA that reached a peak magnitude of $V = 8.86 \pm 0.02$ just 47 seconds after the BATSE trigger. Further optical observations constrained the redshift to between $1.60 \leq z < 2.04$ (Andersen et al. 1999; Kulkarni et al. 1999a), and images taken with the *HST* Space Telescope Imaging Spectrograph (STIS) revealed a host galaxy with $V_0 = 24.25$ (Holland & Hjorth 1999). The burst had a peak fluence of $(5.09 \pm 0.02) \times 10^{-4}$ erg cm^{-2} (Kippen 1999a), which places it in the top 0.3% of the BATSE fluence distribution. This corresponds to a total energy release, assuming isotropy and depending on the details of the adopted cosmology, of between $\approx 3 \times 10^{54}$ and $\approx 4.5 \times 10^{54}$ erg, which is approximately the rest-mass energy of two neutron stars. This amount of energy is difficult to explain using merging compact objects since it would require that the entire rest mass of both objects be converted to gamma radiation with an efficiency of nearly 100%.

GRB 990510 (the Anja burst) was detected by both the *Compton Gamma Ray Observatory* and *BeppoSAX* in the constellation Octans at 8:49:05.95 UT on 1999 May 10. Optical follow-up observations 3.5 hours after the burst revealed an OA with $R \approx 17.5$ (Axelrod et al. 1999). Vreeswijk et al. (1999) found a lower limit for the redshift of $z = 1.619$. A faint galaxy ($V = 28.5 \pm 0.5$) has been detected $0''.066 \pm 0''.009$ from the GRB (Bloom 2000; Fruchter et al 2000). The burst had a peak fluence of $(2.56 \pm 0.09) \times 10^{-5}$ erg cm^{-2} (Kippen 1999b), which places it in the top 9% of the BATSE fluence distribution. This corresponds to a total isotropic energy release, depending on the details of the cosmology, of at least 10^{53} erg, approximately one order of magnitude less than the energy released in GRB 990123.

The light curve for GRB 990123 became steeper approximately two days after the burst (Castro-Tirado et al. 1999; Kulkarni et al. 1999a), while Harrison et al. (1999), Israel

et al. (1999), and Stanek et al. (1999) found that the light curve of GRB 990510 became significantly steeper approximately 1.5 days after the burst. These breaks have been interpreted as evidence that the outflows from the bursts are collimated with opening angles of approximately 5°–10° (Sari et al. 1999; Castro-Tirado et al. 1999). Such models provide a solution to the so-called "energy crisis" of GRBs since, if GRBs are collimated outflows, the total energy requirement drops by factor of between approximately 100 and 1000. This makes the energetics of GRBs consistent with the energetics of supernovae and merging compact objects.

Before GRB 990123 GRB light curves were usually fit by power laws of the form $f_\nu(t) = kt^\alpha$ where k is a normalization constant and α is between approximately -1 and -2. The steepest temporal decay was $\alpha = -2.5$ for the OA associated with GRB 971227 (Djorgovski et al. 1998). The first evidence that the decay of the optical light curve from an OA varies with time came from GRB 990123, where α rapidly steepened from -1.10 ± 0.03 to -1.65 ± 0.06 with the break occurring 2.04 ± 0.46 days after the burst (Kulkarni et al. 1999a). Harrison et al. (1999), Israel et al. (1999), and Stanek et al. (1999) found that the optical light curve for GRB 9900510 exhibited a similar behavior, but with a slow transition between the two regimes. Harrison et al. (1999) used a four-parameter fitting function to find slopes of -0.82 ± 0.02 before the break and -2.18 ± 0.05 after the break with the break occurring 1.20 ± 0.08 days after the burst. However, Stanek et al. (1999) found slopes of -0.76 ± 0.01 before and -2.40 ± 0.02 the break with the break occurring 1.57 ± 0.03 days after the burst; and Israel et al. (1999) found -0.88 ± 0.03 before and -2.68 ± 0.13 after with a break at 1.8 ± 0.2. The latter two groups used a different four-parameter fitting function from Harrison et al. (1999), and the fits formally disagree with each other.

In this paper we collect the published photometry for the OAs associated with GRB 990123 and GRB 990510, examine three fitting functions for broken light curves, and use these fits to constrain physical models for the burst. We investigate the effects of using different fitting functions on determining the time of the break and the slope of the light curve before and after the break. Our goal is to determine reliable light curve parameters for each GRB and to use these parameters to distinguish between different physical models for the nature of each OA. Sect. 2 discusses the three fitting functions that we used to determine the break time, and the slopes of each light curve. Sect. 3 presents our fits to the light curve of GRB 990123's OA and an estimate of the slope of the optical spectrum of the OA. Sect. 4 presents our fits to the light curve of GRB 990510's OA and an estimate of the slope of its optical spectrum. We discuss the effects of the choice of the fitting function on the determination of the break time and slopes of the light curves for each burst. In Sect. 5 we discuss various models for the decay of the light curves, and in Sect. 6 we derive some physical properties for the bursts based on our fits to the light curves. We have written these sections in such a way that they can be used with data from other GRBs.

We have adopted a cosmology with a Hubble parameter of $H_0 = 65$ km s^{-1} Mpc^{-1}, and assumed a density parameter of $\Omega_0 = 0.2$ and no cosmological constant ($\Omega_\Lambda = 0$) throughout this paper.

2. Fitting the light curves

The choice of fitting function is arbitrary, but that choice can affect the determination of the slopes and break time, and thus can influence the interpretation of the light curve. For example, Jensen et al. (2000) find different break times and slopes for the decay of the optical light curve of GRB 000301C depending on whether a broken power law or the continuous function of Stanek et al. (1999) is fit to the data. We have chosen to fit the light curves for the OAs associated with GRB 990123 and GRB 990510 with three fitting functions. The first of these is a broken power law,

$$f_\nu(t) = \begin{cases} f_\nu(t_b)(t/t_b)^{\alpha_1}, & \text{if } t \le t_b \\ f_\nu(t_b)(t/t_b)^{\alpha_2}, & \text{if } t > t_b, \end{cases} \quad (1)$$

where $f_\nu(t)$ is the flux in μJy t days after the burst, and t_b is the time that the light curve made the transition from a slope of α_1 to a slope of α_2. The slope goes as $f_\nu \propto t^{\alpha_1}$ before the break and $f_\nu \propto t^{\alpha_2}$ after the break with an instantaneous transition between the two slopes. This is the simplest form that can be fit to the data, and it can be reduced to two linear functions (i.e., $\ln(f_\nu(t)) = \alpha_1(t/t_b) + \ln(f_\nu(t_b))$ before the break and $\ln(f_\nu(t)) = \alpha_2(t/t_b) + \ln(f_\nu(t_b))$ after the break), which simplifies the fitting process.

The second fitting function is,

$$f_\nu(t) = \frac{f_\nu(t_b)}{1 - e^{-1}} \left(\frac{t}{t_b}\right)^{\alpha_1} \frac{\left[1 - e^{-J}\right]}{J}, \quad (2)$$

where $J = (t/t_b)^{\alpha_1 - \alpha_2}$. This is the continuous function used by Harrison et al. (1999). It is differentiable at $t = t_b$, and is generally more flexible than Eq. (1) is. It is able to model the slow transition between the α_1 and α_2 regimes, which may be more physically realistic than the instantaneous transition that is assumed by the broken power law.

The third fitting function is,

$$f_\nu(t) = \frac{2 f_\nu(t_b)(t/t_b)^{\alpha_2}}{1 + (t/t_b)^{\alpha_2 - \alpha_1}}, \quad (3)$$

which is the same as that used by Stanek et al. (1999) and Israel et al. (1999), except that we have redefined α_1 and α_2 to be consistent with our Eqs. (1) and (2). This function has the same advantages over Eq. (1) that Eq. (2) does.

We wish to stress that none of these functional forms have been derived from any physical principles, and that they are *not* based on any model for the GRB or its OA. The three forms were selected solely because they allow us to parameterize the observed light curves for GRB 990123 and GRB 990510. We used CERN's MINUIT function minimization package, and a chi-square minimization scheme, to simultaneously solve for the four free parameters (α_1, α_2, t_b, and $f_\nu(t_b)$) and to compute the formal 1σ errors in the fit for each parameter.

Table 1. The central wavelengths and photometric zero points for each band pass (from Fukugita et al. 1995).

Filter	λ_0 (Å)	$f_{\nu,0}$ (erg cm^{-1} s^{-1} Hz^{-1})
B	4448	4.02×10^{-20}
V	5505	3.59×10^{-20}
Gunn r	6538	2.96×10^{-20}
R	6588	3.02×10^{-20}
I	8060	2.38×10^{-20}

Table 2. The observed magnitudes (from Castro-Tirado et al. 1999), and the adopted magnitudes and fluxes for the probable host galaxy of GRB 990123.

Filter	Castro-Tirado mag	adopted mag	adopted flux (μJy)
B	24.23 ± 0.10	24.35 ± 0.11	0.729 ± 0.074
V	24.20 ± 0.15	24.25 ± 0.07	0.716 ± 0.046
Gunn r	$\cdots$	24.05 ± 0.07	0.711 ± 0.046
R	23.77 ± 0.10	24.07 ± 0.08	0.709 ± 0.052
I	23.65 ± 0.16	23.83 ± 0.08	0.701 ± 0.052

3. GRB 990123 data

3.1. The photometry

We collected the published optical observations of the OA associated with GRB 990123 from six sources: Castro-Tirado et al. (1999), Fruchter et al. (1999b), Galama et al. (1999a), Holland & Hjorth (1999), Kulkarni et al. (1999a), and Fruchter et al. (1999c). These data consists of 88 observations in the Johnson B-, and V-bands, Kron-Cousins R-, and I-bands, and Gunn r-band. The observations were taken at 19 telescopes over a two month period after the burst. In cases where the same observation was reported in two or more sources, and the quoted magnitudes disagreed with each other, we discarded both observations. This was done because we had no reason to favour one source over the other. In cases where a Gunn r-band magnitude was derived from an R-band magnitude we discarded the derived Gunn r-band data and kept the original R-band data.

We converted the published magnitudes to fluxes using the photometric zero points, $f_{\nu,0}$ from Fukugita et al. (1995). These zero points, and the central wavelengths for each band pass, are listed in Table 1. In order to convert the published photometry to a uniform set of fluxes we applied our own corrections for the light of the probable host galaxy (Holland & Hjorth 1999). In cases where the light from the galaxy had already been subtracted in the published photometry we added it back using the magnitude for the galaxy that was given in the source then subtracted a uniform estimate of the light from the galaxy based on the data of Holland & Hjorth (1999) ($V_0 = 24.25 \pm 0.07$, see Table 2). Castro-Tirado et al. (1999) used $UBVRI$ photometry to determine a spectral energy distribution of $f_\nu \propto \nu^{\beta_{\rm gal}} = \text{constant}$, i.e., $\beta_{\rm gal} \approx 0$, for the host galaxy. Therefore, we converted the Holland & Hjorth (1999) V-band flux for the galaxy to the other band passes using $\text{mag} = V + K_{\rm mag} - K_V - 2.5\beta \log_{10}(\nu_{\rm mag}/\nu_V)$ and $\beta_{\rm gal} = 0$ where K_V and $K_{\rm mag}$ are the photometric zero points of the two band passes. The Castro-Tirado et al. (1999) photometry, and our adopted (dereddened) magnitudes and fluxes for the probable host galaxy, are listed in Table 2. A flat spectrum is consistent with the probable host galaxy being a starburst galaxy.

The Galactic reddening in the direction of GRB 990123 is $E_{B-V} = 0.016 \pm 0.020$ (Schlegel et al. 1998). We assumed that there is no extinction in the host galaxy, but this is probably not a good assumption since it is unlikely that a starburst galaxy is devoid of dust. Reddening due to dust in the host galaxy may result in us underestimating the flux from the host galaxy, and thus overestimating the flux from the OA. To avoid this uncertainty we have fit light curves to each band pass separately since the systematic error in the flux introduced by the unknown extinction will only affect the zero-point of the flux in each bandpass, not the slopes of the light curves.

The fits for each band pass, and each fitting function, are given in Table 3. The uncertainties in the parameters are the formal 1σ errors in the fit and do not include contributions from the covariance between the parameters. The slopes are not strongly correlated with each other, but they are moderately correlated with the location of the break. None of the residuals show any time dependence.

The weighted mean values for each parameter, their standard errors (SE), and the χ^2 per degree of freedom ($\chi^2_{\rm DOF}$) values, are listed in Table 4, for each fitting function. The $BVrRI$ data was used to compute the mean values of the fits to the broken power-law (Eq. (1)) and the $BVrR$ data was used to compute the mean values of the fits to the two continuous functions (Eqs. (2) and (3)). The I-band data were not used when computing the latter two sets of mean values because the fits to the I-band data were not reliable for $t < t_b$. The mean values of α_1 and α_2 agree to within one σ regardless of which function is fit to the data, but the mean value of t_b is significantly smaller for Eq. (2) (Harrison's function) than it is for the other two fitting functions. However, the broken power law (Eq. (1)) gives considerably less scatter in the values of each parameter, particularly t_b, for different band passes than the other two fitting functions do. Therefore, we conclude that the broken power law gives a better fit to the GRB 990123 light curves than either of the continuous functions do. This suggests that the break in the light curve may have been very rapid. The 1σ error in the break time for a broken power law is 0.19 days (see Table 4), which suggests that the break may have occurred over a period of only a few hours. Figs. 1–5 show the data for each band pass with the best-fitting broken power laws superimposed.

To test if the break time depends on the wavelength we computed the probabilities that the break times in each band pass are consistent with the mean break time. If the individual break times are not consistent with the mean then this would suggest that the break between the α_1 and α_2 regimes depends on wavelength, which would be inconsistent with the predictions of the relativistic fireball model. This method makes no assumptions about the physical origin of the light curve. We checked if the break time was dependent on wavelength by evaluating the χ^2

Table 3. The parameters of the best-fitting light curves for the photometry of the OA associated with GRB 990123 in each band pass. Eq. (1) is a broken power law, Eq. (2) is the continuous function of Harrison et al. (1999), and Eq. (3) is the continuous function of Stanek et al. (1999).

Eq.	Filter	α_1	α_2	t_b (days)	$f_\nu(t_b)$ (μJy)	$\chi^2_{\rm DOF}$	DOF
(1)	B	-1.11 ± 0.12	-1.81 ± 0.14	1.57 ± 0.51	9.32 ± 4.38	1.0224	6
	V	-1.28 ± 0.48	-1.58 ± 0.16	1.71 ± 2.20	9.09 ± 17.72	0.7251	8
	Gunn r	-1.11 ± 0.12	-2.01 ± 0.16	2.11 ± 0.83	6.22 ± 3.94	2.6654	4
	R	-1.17 ± 0.30	-1.57 ± 0.11	1.70 ± 0.22	10.74 ± 3.01	0.9111	31
	I	-1.10 ± 0.42	-1.64 ± 0.10	1.36 ± 0.70	15.72 ± 10.83	0.6922	1
(2)	B	-0.83 ± 0.38	-1.81 ± 0.25	0.76 ± 0.93	21.89 ± 34.83	0.5445	6
	V	-0.76 ± 1.82	-1.57 ± 0.19	0.39 ± 0.64	55.90 ± 131.49	0.8296	8
	Gunn r	-0.91 ± 0.24	-2.11 ± 0.31	1.45 ± 1.34	9.34 ± 12.57	3.6172	4
	R	-0.73 ± 1.16	-1.57 ± 0.22	0.54 ± 0.84	40.55 ± 71.25	0.8444	31
	I	$19.07 \pm \cdots$	-1.61 ± 0.06	0.70 ± 0.80	26.00 ± 47.72	0.7975	1
(3)	B	-0.75 ± 0.70	-1.90 ± 0.43	0.92 ± 2.11	17.22 ± 53.45	0.5647	6
	V	-1.12 ± 0.60	-1.71 ± 0.26	1.40 ± 4.29	11.09 ± 48.05	0.8678	8
	Gunn r	-0.87 ± 0.38	-2.25 ± 0.47	1.78 ± 2.46	6.78 ± 14.37	3.9109	4
	R	-0.56 ± 3.23	-1.63 ± 0.68	0.54 ± 2.63	40.64 ± 214.63	0.8722	31
	I	2.55 ± 9.37	-1.62 ± 0.10	0.54 ± 0.24	36.76 ± 30.45	0.7451	1

Table 4. The mean values of α_1, α_2, and t_b for the best fits of Eq. (1) (a broken power law) to the $BVrRI$ data, and of Eq. (2) (Harrison's function) and Eq. (3) (Stanek's function) to the $BVrR$ data, for the OA associated with GRB 990123. P is the probability that each parameter depends on wavelength (see the text).

Eq.	Parameter	Mean $\pm$ SE	χ^2_4	P
(1)	α_1	-1.12 ± 0.08	0.0387	0.0028
	α_2	-1.69 ± 0.06	1.6616	0.8442
	t_b (days)	1.68 ± 0.19	0.1331	0.0297
(2)	α_1	-0.88 ± 0.20	0.0180	0.0033
	α_2	-1.70 ± 0.12	0.9197	0.5697
	t_b (days)	0.61 ± 0.42	0.1814	0.0909
(3)	α_1	-0.91 ± 0.29	0.0658	0.0220
	α_2	-1.83 ± 0.19	0.3748	0.2288
	t_b (days)	1.11 ± 1.30	0.0446	0.0125

statistic for the weighted mean value of t_b. The $\chi^2_{\rm DOF}$ value, and P, the probability that we can reject the null hypothesis that the break time seen in each band pass is consistent with the mean break time (i.e. P is the probability that the break time changes with wavelength), are listed in Table 4. Similar calculations were done for the slopes α_1 and α_2. The P values are all less than 0.9, so we conclude that there is no evidence that the break time, or the slopes, vary with wavelength.

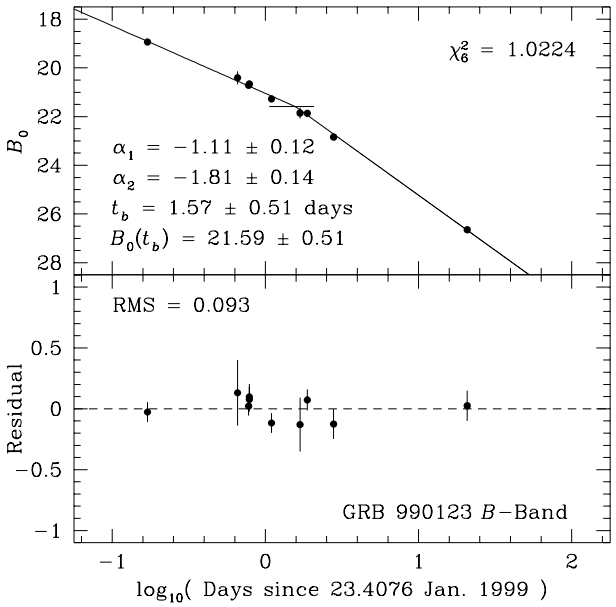

Fig. 1. The upper panel shows the best-fitting broken power law (Eq. (1)) for the GRB 990123 B-band photometry. The horizontal bar shows the 1σ uncertainty in the time of the break. The lower panel shows the residuals in the fit. The residuals are defined as $(B_{\rm fit} - B_{\rm obs})$. The uncertainties in the residuals are the uncertainties in the observed data. The magnitudes have been corrected for Galactic extinction in the direction of GRB 990123, but not for extinction in the host galaxy.

3.2. The spectrum of the optical transient

We have assumed that the OA for GRB 990123 has a power-law spectrum of the form

$$f_\nu(\nu) = f_\nu(10^{15}\,{\rm Hz})\Big(\frac{\nu}{10^{15}\,{\rm Hz}}\Big)^{\beta_{\rm OA}}, \quad (4)$$

where $f_\nu(\nu)$ is the flux, in μJy, at the frequency ν, and $\beta_{\rm OA}$ is the spectral index. The choice of 10^{15} Hz as a reference frequency is arbitrary, but this value gives $\nu/10^{15} \approx 1$, which results in stable fits of the flux data to Eq. (4).

We estimated the spectrum at a series of times by taking the B-, V-, R-, and I-band data in 0.1-day intervals and fitting it to Eq. (4). Only intervals that contained at least three observations spanning two or more filters were considered. Fig. 6 shows the values of $\beta_{\rm OA}$ determined this way. The weighted mean spectral index is $\overline{\beta_{\rm OA}} = -0.750 \pm 0.068$ (SE) with $\chi^2_7 = 0.4711$. The

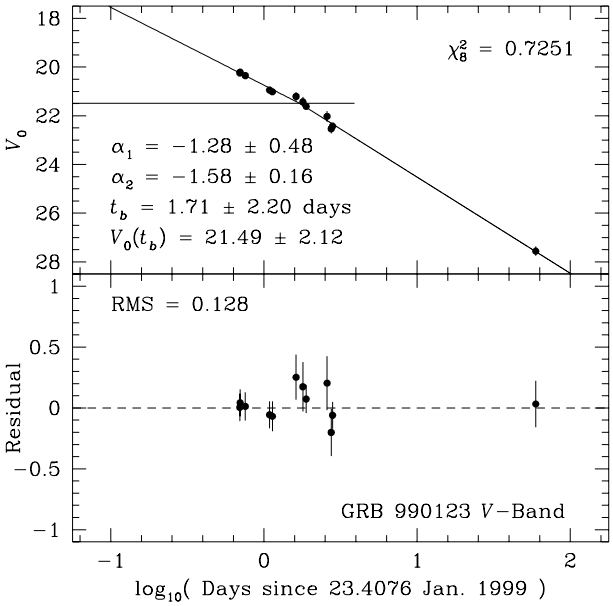

Fig. 2. This figure shows the best-fitting broken power law, and the residuals, for the GRB 990123 V-band data. The large uncertainty in the time of the break ($t_b = 1.71 \pm 2.20$ days) indicates that the data could be well fit by a single power law.

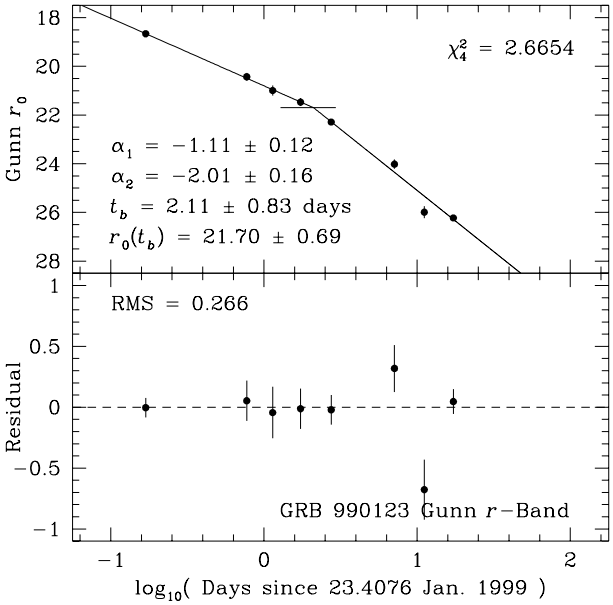

Fig. 3. This figure shows the best-fitting broken power law, and the residuals, for the GRB 990123 Gunn r-band data.

low $\chi^2_{\rm DOF}$ value suggests that we can reject the null hypothesis, that the spectral index is constant with time, at the 17% confidence level. This is too low to be able to reject the null hypothesis, so we conclude that there is no evidence for a variable $\beta_{\rm OA}$. Our value of $\beta_{\rm OA}$ is consistent with the direct measurement of Andersen et al. (1999). They found $\beta_{\rm OA} = -0.69 \pm 0.10$ between 4000 Å $\leq \lambda \leq$ 5700 Å from a spectrum of the OA that was taken 0.8 hours after the burst.

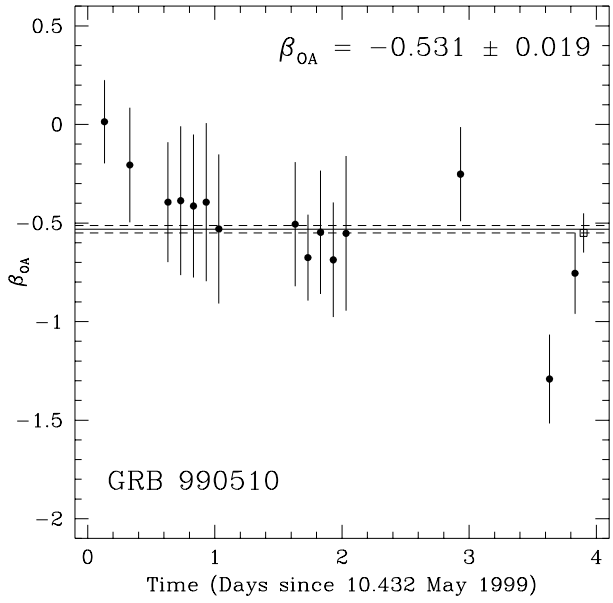

Fig. 4. This figure shows the best-fitting broken power law, and the residuals, for the GRB 990123 R-band data.

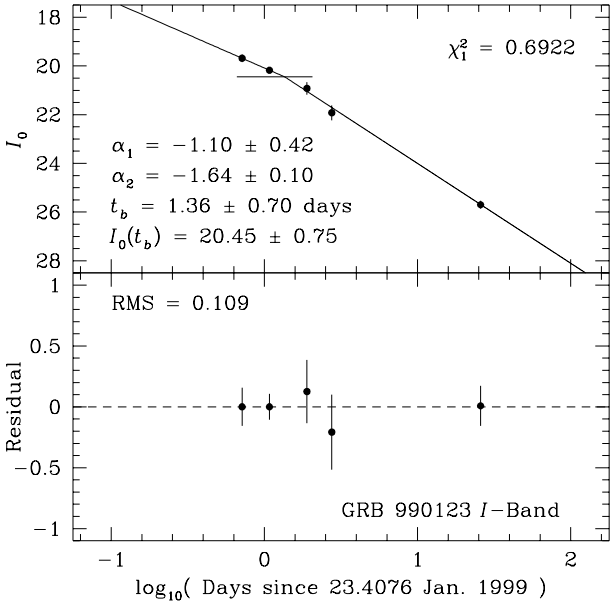

Fig. 5. This figure shows the best-fitting broken power law, and the residuals, for the GRB 990123 I-band data.

4. GRB 990510 data

4.1. The photometry

We collected the published optical observations of the OA associated with GRB 990510 from eleven sources: Beuermann et al. (1999), Covino et al. (1999), Fruchter et al. (1999a), Galama et al. (1999b), Harrison et al. (1999), Marconi et al. (1999a, 1999b), Pietrzyński & Udalski (1999a, 1999b, 1999c), and Stanek et al. (1999). These data consists of 182 observations in the Johnson V-band, and in the Kron-Cousins R-, and I-bands. The observations were taken at seven telescopes up

Table 5. The parameters of the best-fitting light curves for the photometry of the OA associated with GRB 990510 in each band pass. Eq. (1) is a broken power law, Eq. (2) is the continuous function of Harrison et al. (1999), and Eq. (3) is the continuous function of Stanek et al. (1999).

Eq.	Filter	α_1	α_2	t_b	$f_\nu(t_b)$	$\chi^2_{\rm DOF}$	DOF
(1)	V	-0.78 ± 0.12	-2.08 ± 0.20	1.23 ± 0.22	62.72 ± 13.20	1.5183	63
	R	-0.69 ± 0.11	-1.72 ± 0.13	0.87 ± 0.12	96.06 ± 15.50	1.2569	57
	I	-1.16 ± 0.34	-1.73 ± 0.29	1.33 ± 0.66	58.67 ± 41.41	0.9355	50
(2)	V	-0.62 ± 0.19	-2.16 ± 0.29	1.05 ± 0.47	65.54 ± 37.73	0.6395	63
	R	-0.46 ± 0.20	-1.85 ± 0.26	0.70 ± 0.35	114.54 ± 63.24	0.7292	57
	I	-0.67 ± 1.79	-1.84 ± 1.22	0.80 ± 2.26	106.44 ± 351.17	0.8679	50
(3)	V	-0.58 ± 0.23	-2.32 ± 0.37	1.25 ± 0.71	50.70 ± 39.84	0.4218	63
	R	-0.40 ± 0.29	-2.00 ± 0.36	0.81 ± 0.60	96.02 ± 84.48	0.9763	57
	I	-0.51 ± 2.08	-2.02 ± 1.16	0.98 ± 2.85	83.55 ± 310.43	0.8547	50

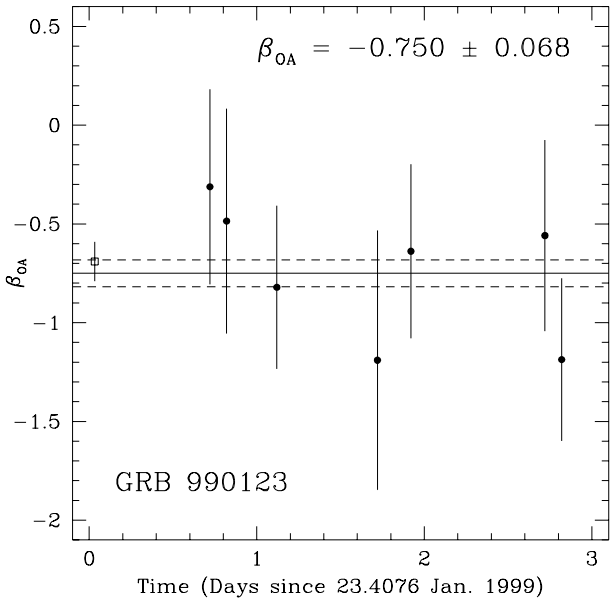

Fig. 6. This figure shows $\beta_{\rm OA}$, the spectral index of the light from the OA associated with GRB 990123 (filled circles), as a function of time. The error bars are defined as $\sigma_\beta = \sqrt{\sum_{i=1}^{N} (\sigma_{f,i}/f_i)^2}$ where $\sigma_{f,i}$ is the uncertainty in each flux value, f_i. The solid line shows the weighted mean value of $\beta_{\rm OA}$ while the dashed lines show the 1σ uncertainty in $\overline{\beta_{\rm OA}}$. The open square shows the Andersen et al. (1999) spectral value. The data are consistent with a constant $\beta_{\rm OA}$ of -0.750 ± 0.068. There is no evidence that $\beta_{\rm OA}$ varies with time.

to 40 days after the burst. The published magnitudes were converted to fluxes in the same manner as described in Sect. 3.1. No corrections were made for a host galaxy since no host galaxy has been observed for this burst to a limiting magnitude of $R = 27.6$ (Beuermann et al. 1999)[1]. The Galactic reddening in the direction of GRB 990510 is $E_{B-V} = 0.203 \pm 0.020$ (Schlegel et al. 1998). We assumed that the extinction in the host galaxy was $A_V = 0$.

[1] Recently Bloom (2000) and Fruchter et al (2000) reported evidence for a faint ($V = 28.5 \pm 0.5$) host galaxy. This corresponds to a flux of ≈ 0.014 μJy in the V band, which is not sufficient to affect the results of our fits.

The fits for each band pass, and each fitting function, are given in Table 5. The uncertainties in the parameters are the formal 1σ errors in the fits and do not include contributions from the covariance between the parameters. The residuals for all three fitting functions show some structure near the location of the break. This suggests that none of the three fitting functions which we used in this paper accurately reproduce the temporal behavior of the light curve during the transition from the α_1 regime to the α_2 regime. The last two V-band observations, and the last R-band observation, were derived from images taken with the *HST*/STIS and were transformed from the 50CCD (clear) aperture to the V and R bands assuming a spectral index of $\beta_{\rm OA} = -0.6$ (Fruchter et al. 1999a). These observations were taken approximately one month after the other observations, so the large residuals for these three data points may be due to a change in the shape of the OA's spectrum during that period, or systematic uncertainties in transforming the 50CCD magnitudes to VR magnitudes.

The weighted mean values for each parameter, their standard errors, and the $\chi^2_{\rm DOF}$ values are listed in Table 6 for the fits to each fitting function. The mean values of α_1, α_2, and t_b agree to within approximately 1.5σ regardless of which function is fit to the data. However, there are systematic variations in the residuals of the fits of Eq. (1) (the broken power law) to the V- and R-band data. This indicates that one of the continuous functions (Eq. (2) or (3)) provides a better fit to the data than the broken power law (Eq. (1)) does, which in turn suggests that the break in the light curve was not nearly instantaneous as was the case with GRB 990123, but may have occurred over a period of approximately one day. Eq. (2) (Harrison's function) gives the smallest residuals, and the least scatter in the values of the parameters in different band passes, so we have adopted it as the best fitting function. The P values in Table 6 are all less than 0.7, so we conclude that there is no evidence for any variation in α_1, α_2, or t_b with wavelength. Figs. 7–9 show the data for each band pass with the best-fitting continuous functions superimposed.

4.2. The spectrum of the optical transient

We estimated the spectral index for the OA associated with GRB 990510 in the same way as we did for the OA associated

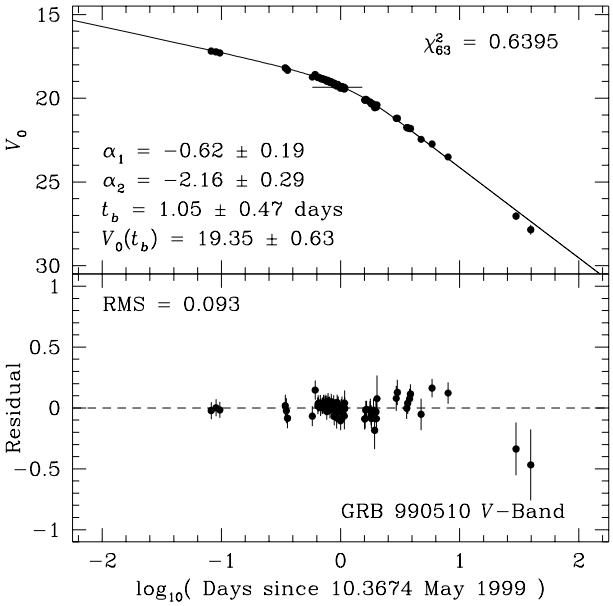

Fig. 7. The upper panel shows the best-fitting continuous function (Eq. (2), Harrison's function) for the GRB 990510 V-band photometry. The horizontal bar shows the 1σ uncertainty in the time of the break. The lower panel shows the residuals in the fit in the sense $(V_{\rm fit} - V_{\rm obs})$. The magnitudes have been corrected for Galactic extinction in the direction of GRB 990510.

Table 6. The mean values of α_1, α_2, and t_b for the best fits of Eq. (1) (a broken power law), Eq. (2) (Harrison's function), and Eq. (3) (Stanek's function) to the VRI data for the OA associated with GRB 990510. P is the probability that each parameter depends on wavelength (see the text).

Eq.	Parameter	Mean ± SE	χ^2_3	P
(1)	α_1	-0.75 ± 0.18	1.8114	0.5957
	α_2	-1.81 ± 0.10	1.1878	0.6951
	t_b	0.96 ± 0.10	1.1913	0.6962
(2)	α_1	-0.54 ± 0.14	0.1707	0.1569
	α_2	-1.98 ± 0.19	0.3239	0.2767
	t_b	0.82 ± 0.28	0.1784	0.1634
(3)	α_1	-0.51 ± 0.18	0.1182	0.1115
	α_2	-2.15 ± 0.25	0.1986	0.1801
	t_b	0.99 ± 0.45	0.1120	0.1060

with GRB 990123 (see Sect. 3.2). Fig. 10 shows the values of $\beta_{\rm OA}$ that were determined in this manner. The weighted mean spectral index is $\beta_{\rm OA} = -0.531 \pm 0.019$ (SE) with $\chi^2_{14} = 1.6598$, which suggests that we can reject the hypothesis that the spectral index is constant with time at the 95% confidence level. Our mean value for $\beta_{\rm OA}$ is consistent (within 1.5σ) with the value obtained by Beuermann et al. (1999) using long-slit spectrophotometry 3.9 days after the burst. They found $\beta_{\rm OA} = -0.55 \pm 0.10$ in the interval 4900 Å $\leq \lambda \leq$ 9000 Å.

Our result is consistent with the spectral index increasing from $\beta_{\rm OA} \approx 0$ at the time of the burst to $\beta_{\rm OA} \approx -0.6$ at the time of the break in the light curve ($t_b = 0.82 \pm 0.28$ days after the burst). After the break the spectral index stays constant at

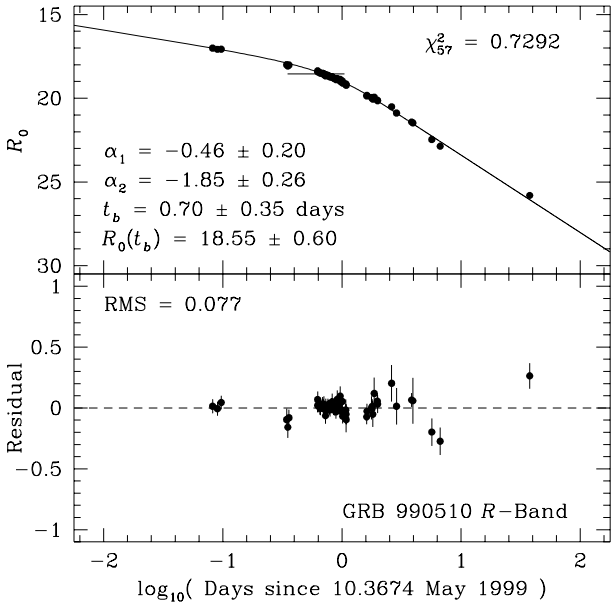

Fig. 8. This figure shows the best-fitting continuous function (Eq. (2)), and the residuals, for the GRB 990510 R-band data.

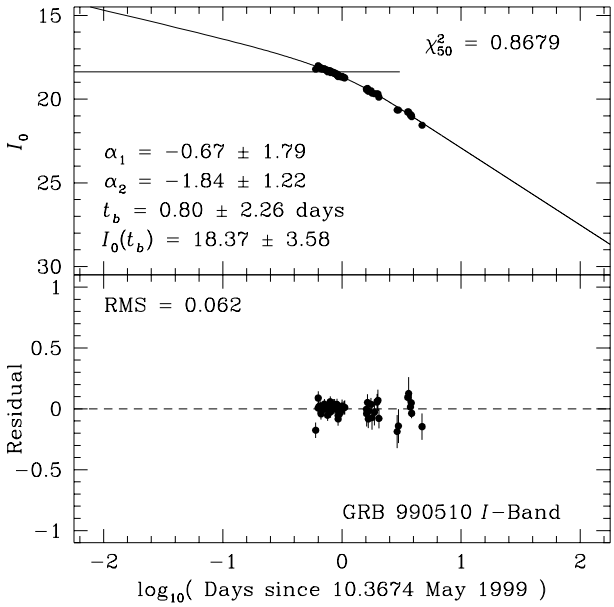

Fig. 9. This figure shows the best-fitting continuous function (Eq. (2)), and the residuals, for the GRB 990510 I-band data. The large uncertainty in the time of the break ($t_b = 0.80 \pm 2.26$ days) indicates that the data can be well fit by a single power law.

$\beta_{\rm OA}$ of -0.62 ± 0.06, which is consistent with the Beuermann et al. (1999) result. We find $\beta_{\rm OA} = -1.29 \pm 0.23$ 3.6 days after the burst. This is inconsistent with the Beuermann et al. (1999) data, but is consistent with the spectral index continuing to increase after the break in the light curve occurred. However, we believe that the direct measurement of Beuermann et al. (1999) is more reliable than our indirect measurements of $\beta_{\rm OA}$ so we conclude that it is unlikely that the spectral index continues to increase after the break.

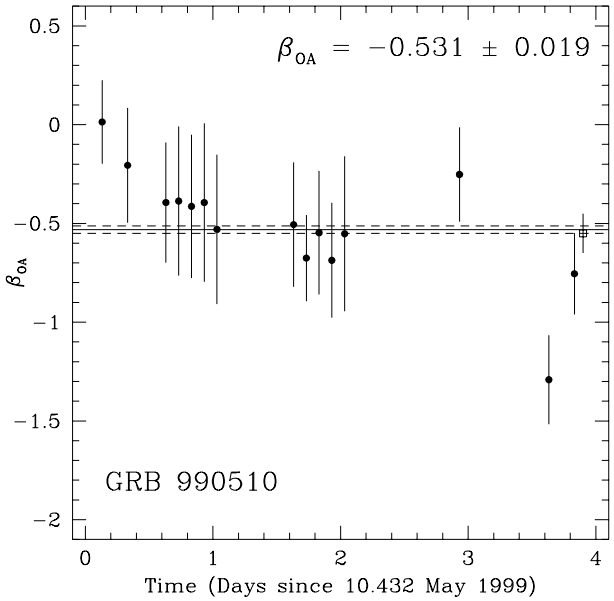

Fig. 10. This figure shows $\beta_{\rm OA}$, the spectral index of the light from the OA associated with GRB 990510 (filled circles), as a function of time. The solid line shows the weighted mean value of $\beta_{\rm OA}$ while the dashed lines show the 1σ uncertainty in $\overline{\beta_{\rm OA}}$. The open square shows the Beuermann et al. (1999) spectrophotometric data. The data are inconsistent with a constant $\beta_{\rm OA}$ at the 95% confidence level (92% confidence level if the spectrophotometric datum is included).

5. Models

The generic model for an OA associated with a GRB is a fireball expanding relativistically into an ambient medium of number density n, and decelerating as it sweeps up matter. The shock between the fireball and the medium accelerates electrons to relativistic energies, and gives them a power-law distribution of energies, $N(\gamma) \propto \gamma^{-p}$. The total energy in the electrons is parameterized by ϵ_e, the ratio between the energy in electrons and the energy in nucleons. Similarly, the magnetic field strength is parameterized by ϵ_B, the ratio of the comoving field energy density and the post-shock nucleon energy density (e.g. Wijers & Galama 1998).

At a given instant in the fireball evolution the instantaneous spectrum of the OA is determined by the local conditions in the shock region. In particular, the electron energy index p determines the spectral slope of the synchrotron emission $f_\nu \propto t^\alpha \nu^\beta$, e.g., through the relation $\beta = -(p-1)/2$. Following Sari et al. (1998), we have, for the fast cooling regime,

$$f_\nu = \begin{cases} (\nu/\nu_c)^{-1/2} f_{\nu_m}, & \nu_c < \nu < \nu_m, \\ (\nu_m/\nu_c)^{-1/2} (\nu/\nu_m)^{-p/2} f_{\nu_m}, & \nu > \nu_c, \end{cases} \quad (5)$$

while in the slow cooling regime we have

$$f_\nu = \begin{cases} (\nu/\nu_m)^{-(p-1)/2} f_{\nu_m}, & \nu_m < \nu < \nu_c, \\ (\nu_c/\nu_m)^{-(p-1)/2} (\nu/\nu_c)^{-p/2} f_{\nu_m}, & \nu_c < \nu. \end{cases} \quad (6)$$

The synchrotron peak frequency, ν_m, the flux at that frequency f_{ν_m}, and the frequency ν_c corresponding to the electron Lorentz factor that separates the fast cooling electrons from the slow cooling ones, all depend on the model parameters and the fireball geometry (spherical or collimated). Explicit expression for these cases can be found in Sari et al. (1998), Wijers & Galama (1998) (spherical), and Rhoads (1999) (jet). We do not consider the spectrum below ν_c and ν_m in the fast and slow cooling regimes, respectively, as this is not of interest in the present discussion. The time dependence of ν_m, ν_c, and f_{ν_m} is different in spherical and collimated models and has been discussed by e.g. Rhoads (1999; see also Sari et al. 1999).

For a collimated outflow in an ambient medium of constant number density n, we have (Rhoads 1999)

$$\nu_m = 3.66 \cdot 10^{16} x_p \epsilon_e^2 \epsilon_B^{1/2} \left(\frac{E_{52}}{\theta_0} \right)^{1/2} \frac{(1+z)^{1/2}}{t_d^{3/2}} \,\mathrm{Hz}, \quad (7)$$

$$\nu_c = 1.04 \cdot 10^{11} \epsilon_B^{-3/2} E_{52}^{-2/3} n^{-5/6} \,\mathrm{Hz}, \text{ and} \quad (8)$$

$$f_{\nu_m} = 1.8 \cdot 10^{-2} (1+z) \epsilon_B^{1/2} \phi_p \left(\frac{E_{52}}{\theta_0^2} \right) n^{1/2} \frac{d_L}{4.82\,\mathrm{Gpc}} \,\mathrm{Jy}. \quad (9)$$

Here, x_p is the dimensionless frequency at maximum flux and ϕ_p is the dimensionless flux at that frequency (Wijers & Galama 1998). These are determined by the index p of the electron energy distribution. The burst energy in units of 10^{52} erg is denoted by E_{52}, θ_0 is the half angle of the collimated jet, t_d is the time in days, and d_L is the luminosity distance to the burst.

To connect the optical observations in a given band pass directly to the model parameters we rewrite, for example, Eq. (6) as

$$\nu^{(p-1)/2} f_\nu = \nu_m^{(p-1)/2} f_{\nu_m} \quad (10)$$

for $\nu_m < \nu < \nu_c$ in the slow cooling regime, while for $\nu > \nu_c$ we would have

$$\nu^{p/2} f_\nu = \left(\frac{\nu_m}{\nu_c} \right)^{(p-1)/2} \nu_c^{p/2} f_{\nu_m}. \quad (11)$$

Similar expression may be obtained in the fast cooling regime. Combining ν_m and f_{ν_m} according to Eq. (10), or ν_m, ν_c, and f_{ν_m} according to Eq. (11), depending on the frequency range of interest, allows us to directly connect the observations at a given frequency to the model parameters. The general formula that is obtained this way is complicated but may be simplified in specific cases (see Eq. (15)).

The properties of the observed light curve of the OA, such as the rate of decay α, are primarily determined by the hydrodynamic evolution of the fireball. In particular, spherical and collimated bursts give rise to different forms of light curves. The adiabatic evolution of the Lorentz factor, Γ, of the fireball is given by (Sari et al. 1998; Sari & Piran 1999)

$$\Gamma = 6.65 \left(\frac{E_{52}}{n} \right)^{1/8} t_d^{-3/8}, \quad (12)$$

A spherical outflow generally results in a uniformly decaying light curve that can have modest breaks which are due to the

Table 7. The electron energy index before, p_1, and after, p_2, the break in the light curve, and the size of the break, $\Delta\alpha$, inferred from the observations of GRB 990123 for the three models discussed in the text. The observed values are given for comparison. The observed value of p is computed from our observed value of $\overline{\beta_{\rm OA}} = -0.750 \pm 0.068$.

	Spherical + non-relativistic	θ_0 constant	Sideways expansion	Observed
p_1	$1 - 4\alpha_1/3 = 2.49 \pm 0.11$	$1 - 4\alpha_1/3 = 2.49 \pm 0.11$	$1 - 4\alpha_1/3 = 2.49 \pm 0.11$	2.50 ± 0.14
p_2	$(21 - 10\alpha_2)/15 = 2.53 \pm 0.04$	$-4\alpha_2/3 = 2.25 \pm 0.06$	$-\alpha_2 = 1.69 \pm 0.06$	2.50 ± 0.14
$\Delta\alpha$	$-(\alpha_1 + 3/5) = 0.52 \pm 0.06$	$3/4$	$1 - \alpha_1/3 = 1.37 \pm 0.02$	0.57 ± 0.10

different time evolution of the characteristic frequencies ν_m and ν_c (Sari et al. 1998). A pronounced break in the light curve may be observed in a spherical outflow that becomes non-relativistic, but requires the ambient medium to be denser, by several orders of magnitude, than generally expected (Wijers et al. 1997; Dai & Lu 1999). The steepening of the light curve in the case of a spherical fireball entering a non-relativistic phase can be shown to be $\Delta\alpha = (\alpha_1 - \alpha_2) = -(\alpha_1 + 3/5)$.

Collimated outflows, on the other hand, give rise to a light curve that resembles a broken power-law which becomes steeper between several hours and several days after the gamma-ray event. There are two general possibilities.

1. There is a collimated outflow with a fixed opening angle θ_0. When Γ decreases to $\Gamma \approx 1/\theta_0$, the light curve steepens. This steepening occurs because after the outflow has decelerated the observer only receives radiation emitted within the collimated beam (Mészáros & Rees 2000; Kulkarni et al. 1999a). The amount of steepening is $\Delta\alpha = 3/4$. This is a purely geometrical effect, so the intrinsic properties of the fireball are not affected by the transition to the $\Gamma < 1/\theta_0$ regime.
2. The collimated outflow may expand sideways as well as radially (e.g. Rhoads 1999; Panaitescu & Mészáros 1998). Initially, the relativistic beaming dominates over the sideways expansion, but when sideways expansion sets in, the radial expansion essentially comes to a halt, which results in a steepening of the light curve. Simple analytic estimates show that this steepening is $\Delta\alpha = 1 - \alpha_1/3$ (Rhoads 1999), while detailed numerical simulations show that the steepening is expected to be more gradual both in time and slope (Moderski et al. 2000).

6. Interpretation

6.1. GRB 990123

The synchrotron peak frequency, ν_m, was most likely in the radio already on 1999 January 24.65 (Galama et al. 1999a), implying that the electrons were already in the slow cooling regime. The flux at frequency ν would then be given by Eq. (10). The isotropic energy of the burst, E_{52}, that was estimated from the gamma-ray data, is $E_{52} = 338 \pm 1$ at the observed redshift of $z = 1.6$.

The spectral index that we determined for GRB 990123, $\beta = -0.750 \pm 0.068$, corresponds to an electron index of $p = 2.500 \pm 0.136$. There is no evidence for variations in β across the break in the light curve, so we can conclude that p is constant during the observed evolution of the light curve. The reliability of β and p obtained in this way is questionable, however, as the effect of extinction on β is unknown. The light curve decay indices, α_1 and α_2, on the other hand, are also a function of p, and are not affected by extinction. Therefore, we have elected to use our fits to the measured light curves to obtain the electron index, and use that to infer the spectral index.

In Table 7 we compare the electron energy index that we calculate from the light curve indices using three different models and assuming that the ambient medium has a constant density. During the initial phase, all models look spherical to the observer, hence p is the same for all of them. After the break in the light curve, different models give different relationship between the light curve decay rate and p, as indicated in Table 7. The last line in Table 7 gives the size of the break that is predicted by each model and should be compared to the observed size of the break, $\Delta\alpha = 0.57 \pm 0.10$. A spherically expanding fireball entering a non-relativistic regime at the time of light curve break gives the best overall agreement with the data (see also Dai & Lu 1999; Wang et al. 1999). That interpretation, however, does have problems in accounting simultaneously for the optical and radio properties of the burst (Kulkarni et al. 1999b). It is worth noting that the sideways expanding jet predicts a break in the light curve of $\Delta\alpha = 1.37$, which is more than twice the size of the observed break.

Our preferred model in interpreting this burst is that of a collimated outflow of a fixed opening angle. The main reason for this choice is the model's ability to self-consistently account for the observations at *all* wavelengths. If we accept the constant θ_0 model as the best description of GRB 990123, we can deduce the remaining model parameters. Evaluating Eq. (12) at $t_d = t_b = 1.68$, and using $E_{52} = 338$, we find that the Lorentz factor of the fireball at the time of the break is

$$\Gamma = 5.47 \left(\frac{E_{52}}{n} \right)^{1/8} \approx 11 n^{-1/8}. \quad (13)$$

Therefore, interpreting the break in the light curve as a geometrical effect, we find the opening angle of the collimated outflow to be

$$\theta_0 \approx \frac{1}{\Gamma} \approx \frac{1}{11} n^{1/8} \approx 5^\circ n^{1/8}, \quad (14)$$

which enables us to eliminate the opening angle from the expressions for ν_m and f_{ν_m} (Eqs. (7) and (9)). The opening angle is weakly dependent on the number density of the medium where

the burst occurred. Typical number densities in star-forming regions, for example, can vary from $n \approx 1$ to $n \gtrsim 1000$. However, this range of number densities corresponds to opening angles of $5^\circ \lesssim \theta_0 \lesssim 12^\circ$, so the amount of collimation does not depend strongly on the density of the ambient medium.

The fireball evolution is independent of colour, so observations in different bands passes should give identical results when evaluating the left hand side of Eq. (10). Using the data for Eq. (1) (the broken power law) in Table 3 at the time of the break in the corresponding light curve, averaging over all five band passes, and rearranging, we obtain

$$\epsilon_e^{p-1}\epsilon_B^{(p+1)/4}E_{52}^{(p+1)/4}n^{-(p-9)/32} \approx 1.34 \cdot 10^{-2}. \quad (15)$$

We have retained p in the exponents of the model parameters to show their explicit appearance, but used $p = 2.37$ (the mean of p_1 and p_2 for the constant θ_0 model), to evaluate the right hand side. Note that the above equation constrains four independent model parameters, but the isotropic energy of the burst, $E_{52} = 338 \pm 1$, can be determined directly from observations, so only three parameters remain undetermined.

An additional expression can be obtained using the $2 - 10$ keV X-ray data obtained on 1999 January 24.2 (Heise et al. 1999). At that time the cooling frequency was less than the frequency of the X-rays ($\nu > \nu_c$), so Eq. (11) applies. Evaluating the left-hand side of Eq. (11) using the X-ray observations we find

$$\epsilon_e^{p-1}\epsilon_B^{(p-5)/4}n^{-(p-9)/32-5/6}E_{52}^{(3p-5)/12} = 2089, \quad (16)$$

and combining the optical and X-ray results gives

$$\epsilon_B^{3/2}n^{5/6} \approx 1.33 \cdot 10^{-7}. \quad (17)$$

This gives $\epsilon_B \approx 2.6 \cdot 10^{-5}$ and $\epsilon_e \approx 0.79$ if $n = 1$ cm^{-3}, or $\epsilon_B \approx 5.6 \cdot 10^{-7}$ and $\epsilon_e \approx 2.94$ if $n = 1000$ cm^{-3}. An additional relation is needed in order to determine n independently.

An alternative, but related interpretation is collimated outflow in an ambient medium with a number density distribution of the form $n(r) \propto r^{-\delta}$ (see Panaitescu et al. 1998: Mészáros et al. 1998). Here, $\delta = 0$ represents a homogeneous distribution, while $\delta = 2$ represents a distribution characteristic of a pre-existing stellar wind. The light curve decay rates will be steeper in a wind distribution than if the density is constant, and the break in the light curve will be less pronounced. In general $\Delta\alpha = (3 - \delta)/(4 - \delta)$. This reproduces $\Delta\alpha = 3/4$ when $\delta = 0$, as discussed above, but gives $\Delta\alpha = 0.5$ for a stellar wind density distribution ($\delta = 2$).

Interpreting the burst using this model we obtain $\delta = 1.67 \pm 0.54$, which is consistent with a stellar wind density distribution. This model adds δ as a new parameter, but constrains β, since the spectral index is now fixed by the light curve decay rates (α_1 and α_2) and δ. We obtain $\beta = -0.51 \pm 0.14$, which is marginally consistent with the spectral index inferred from the data, resulting in $p = 2.02 \pm 0.28$. The other model parameters, discussed above are similar to what is found in the $\delta = 0$ case.

6.2. GRB 990510

GRB 990510 was a strong burst, although none of its observed properties were extraordinary in any way (Wijers et al 1999). The lower limit to its redshift is $z = 1.619 \pm 0.002$ (Vreeswijk et al. 1999), and the isotropic energy release was $E_{52} = 17 \pm 1$. The afterglow was the first to show a smooth break in the light curve rather than a sharp break at a fixed point in observer time.

The measured light curve decay index before the break, $\alpha_1 = -0.54 \pm 0.14$, is too small to be explained by adiabatic fireball scenarios as it leads to a value for the electron energy index, $p < 2$, that is too small. It is, however, consistent with a radiative fireball (e.g. Sari et al. 1998). In that case the light curve is predicted to decay as $t^{-4/7}$ with a corresponding spectral index of $\beta = -1/2$. These values are both independent of p, and are in good agreement with the observed value of α_1, and the value of β that we inferred from the light curves. After the initial radiative stage, the fireball evolves to the more commonly observed adiabatic phase.

In Table 8 we compare the electron energy index, p, calculated from the observed value of α_1 for the three models considered in the previous section. As already mentioned the initial slow decay is incompatible with the requirement that the electron population have a finite energy, i.e., electron energy indices of $p < 2$ correspond to infinite energy, and only the sideways expanding jet model is consistent with the behavior of the light curve at late time. This model also gives good agreement for the size of the break in the observed light curve, $\Delta\alpha = 1.44 \pm 0.17$. The smooth break in the light curve (see also Stanek et al. 1999; Israel et al. (1999), and Harrison et al. 1999), further supports that interpretation (Moderski et al. 2000). The late time spectral index, calculated from p_2, is $\beta_{\rm OA} = -0.49 \pm 0.10$. This is in good agreement with the value determine from spectrophotometry ($\beta_{\rm OA} = -0.55 \pm 0.10$, Beuermann et al. 1999), and the mean value that we calculated from the light curve ($\overline{\beta_{\rm OA}} = -0.53 \pm 0.02$). Therefore, the sideways expanding jet, with a radiative initial phase, is our preferred model.

Applying an analysis similar to the one that we did for GRB 990123, we obtain an opening angle of $\theta_0 \approx 5^\circ n^{1/8}$, which is consistent with the opening angle derived by Harrison et al. (1999) for GRB 990510 and the opening angle that we derived for GRB 990123. In principle it is possible to derive ϵ_e and ϵ_B in the same manner that we did for GRB 990123. However, to do this we need an observation of the flux at $\nu > \nu_c$, and, unfortunately, there are no observations in the literature at these frequencies. Therefore, we are not able to break the degeneracy between ϵ_e, ϵ_B, and n that is seen in Eq. (15).

7. Conclusions

It is possible to learn a great deal about the nature of a GRB, and the environment where the burst occurred, from the optical light curve of the burst's OA. However, it is important that the decaying light curve be well-sampled in order to accurately determine the time and shape of the break, as well as the slope of the light curve before and after the break.

Table 8. Predicted parameters for three models for gamma-ray bursts and the GRB 990510 observations.

	Spherical + non-radiative	θ_0 constant	Sideways expansion	Observed
p_1	$1-4\alpha_1/3 = 1.72 \pm 0.19$	$1-4\alpha_1/3 = 1.72 \pm 0.19$	$1-4\alpha_1/3 = 1.72 \pm 0.19$	1.35 ± 0.14
p_2	$(21-10\alpha_2)/15 = 2.72 \pm 0.13$	$-4\alpha_2/3 = 2.64 \pm 0.25$	$-\alpha_2 = 1.98 \pm 0.19$	2.24 ± 0.12
$\Delta\alpha$	$-(\alpha_1+3/5) = -0.06 \pm 0.14$	$3/4$	$1-\alpha_1/3 = 1.18 \pm 0.14$	1.44 ± 0.24

GRB 990123 and GRB 990510 are the first two GRBs for which breaks have been observed in their optical light curves. We have collected all of the published photometry for these two bursts and determined the time of the break and the slopes of these light curves before and after the break using three different fitting functions. We also estimated the spectral indices of each OA from near-simultaneous broad-band photometry. These parameters were used to constrain models for the nature of each burst. Our results suggest the following.

1. Both GRB 990123 and GRB 990510 exhibit breaks in their optical light curves at times between approximately one and two days after the bursts. There is no evidence that the time of the break depends on frequency. The break in GRB 990123's optical light curve appears to have occurred very fast, perhaps over a period of less than five hours. This is in sharp contrast to the break in the optical light curve for GRB 990510, which appears to have occurred slowly over approximately one day.
2. Unlike GRB 000301C (Jensen et al. 2000) the parameters of the light curve (α_1, α_2, and t_b) for GRB 990123 and GRB 990510 are not strongly dependent on the fitting function. This means that our interpretations are not strongly dependent on the type of fitting function used to derive the slopes and break time. However, the choice of fitting function can influence the interpretation of the light curve for some GRBs.
3. Our favoured interpretation for the optical light curve of GRB 990123 is that the afterglow was collimated with a fixed opening angle of $\theta_0 \approx 5^\circ$. Therefore, the observed break in the light curve is a geometric effect that occurs when the relativistic expansion of the fireball slows to $\Gamma \approx 1/\theta_0$. This model reduces the energy released by the GRB by a factor of ≈ 300 to $E_{52} = 1.1$, which corresponds to the conversion of ≈ 0.01 Solar masses of material to gamma radiation. The magnetic field strength is $\epsilon_B \approx 2.6 \times 10^{-7}$ if the local number density is ≈ 1 cm^{-3} and $\epsilon_B \approx 5.6 \times 10^{-5}$ if the local number density is ≈ 1000 cm^{-3}. This is well below the equipartition energy.
4. The OA's light curve for GRB 990510 is consistent with a collimated outflow that is initially radiative. The transition to an adiabatic phase, and the onset of a sideways expansion of the jet, occurred near the time of the break. The opening angle was $\theta_0 \approx 5^\circ$ at that time, the same as GRB 990123. We are unable to estimate reliably the magnetic field strength because no measurements are available of the flux at frequencies above ν_c, the electron cooling frequency.

We have investigated several models for GRB 990123 and GRB 990510 and find that the OAs for these two bursts can not be explained with a single model. This suggests that the local environment where a GRB occurs plays an important role in determining the evolution of the fireball, and the observed light curve of the OA. We note, however, that the uncertainties in determining the break time and slopes of the light curves make it difficult to unambiguously determine the physics of the optical afterglow and its environment.

Acknowledgements. This research was supported by the Danish Natural Science Research Council (SNF), the Icelandic Research Council and the University of Iceland Research Fund. We wish to thank the referee for several useful comments that allowed us to improve the manuscript.

References

Akerlof C.W., McKay T.A., 1999, GCN Circ. 205
Akerlof C., Balsano R., Barthelmy S., et al., 1999, Nat. 398, 400
Andersen M.I., Castro-Tirado A.J., Hjorth J., et al., 1999, Sci 283, 2075
Axelrod T., Mould J., Schmidt B., 1999, GCN Circ. 315
Beuermann K., Hessman F.V., Reinsch K., et al., 1999, A&A 352, L26
Bloom J.S., 2000, GCN Circ. 756
Castro-Tirado A.J., Rosa Zapatero-Osorio M., Caon N., et al., 1999, Sci 283, 2069
Covino S., Lazzati D., Ghisellini G., et al., 1999, GCN Circ. 330
Dai Z.G., Lu T., 1999, ApJ 519, L155
Djorgovski S.G., Kulkarni S.R., Bloom J.S., et al., 1998, ApJ 508, L17
Fruchter A.S., Hook R., Pian E., 2000, GCN Circ. 757
Fruchter A.S., Ferguson H., Pepper J., et al., 1999a, GCN Circ. 386
Fruchter A.S., Thorsett S.E., Metzger M.R., et al., 1999b, ApJ 519, L13
Fruchter A.S., Thorsett S.E., Pian E., 1999c, GCN Circ. 354
Fukugita M., Shimasaku K., Ichikawa T., 1995, PASP 107, 945
Galama T.J., Briggs M.S., Wijers R.A.M.J., et al., 1999a, Nat. 398, 394
Galama T.J., Vreeswijk P.M., Rol E., et al., 1999b, GCN Circ. 313
Harrison F.A., Bloom J.S., Frail D.A., et al., 1999, ApJ 523, L121
Heise J., DeLibero C., Daniele M.R., et al., 1999, IAU Circ. 7099
Holland S., Hjorth J., 1999, A&A 344, L67
Israel G.L., Marconi G., Covino S., et al., 1999, A&A 348, L5
Jensen B.L., Fynbo J.U., Gorosabel J., et al., 2000, submitted to A&A, astro-ph/0005609
Kippen R.M., 1999a, GCN Circ. 224
Kippen R.M., 1999b, GCN Circ. 322
Kulkarni S.R., Djorgovski S.G., Odewahn S.C., et al., 1999a, Nat 398, 389
Kulkarni S.R., Frail D.A., Sari R., et al., 1999b, ApJ 522, L97
Marconi G., Israel G.L., Lazzati D., Covino S., Ghisellini G., 1999a, GCN Circ. 329
Marconi G., Israel G.L., Lazzati D., Covino S., Ghisellini G., 1999b, GCN Circ. 332

Mészáros P., Rees M.J., 2000, ApJ 530, 292
Mészáros P., Rees M.J., Wijers R.A.M.J., 1998, ApJ 499, 301
Moderski R., Sikora M., Bulik T., 2000, ApJ 529, 151
Panaitescu A., Mészáros P., 1998, In: Paul J., Montmerle T., Aubourg A.E. (eds.) 19th Texas Symposium on Relativistic Astrophysics and Cosmology, p. 44
Panaitescu A., Mészáros P., Rees M.J., 1998, ApJ 503, 314
Pietrzyński G., Udalski A., 1999a, GCN Circ. 328
Pietrzyński G., Udalski A., 1999b, GCN Circ. 319
Pietrzyński G., Udalski A., 1999c, GCN Circ. 316
Piro L., 1999, GCN Circ. 199
Rhoads J.E., 1999, ApJ 525, 737
Sari R., Piran T., 1999, ApJ 520, 641
Sari R., Piran T., Halpern J.P., 1999, ApJ 519, L17
Sari R., Piran T., Narayan R., 1998, ApJ 497, L17
Schlegel D.J., Finkbeiner D.P., Davis M., 1998, ApJ 500, 525
Stanek K.Z., Garnavich P.M., Kaluzny J., Pych W., Thompson I., 1999, ApJ 522, L39
Vreeswijk P.M., Galama T.J., Rol E., et al., 1999, GCN Circ. 324
Wang X.Y., Dai Z.G., Lu T., 1999, MNRAS 317, 170
Wijers R.A.M.J., Galama T., 1998, ApJ 523, 177
Wijers R.A.M.J., Vreeswijk P.M., Galama T.J., et al., 1999, ApJ 523, L33
Wijers R.A.M.J., Rees M.J., Mészáros P., 1997, MNRAS 288, L51